Check for updates

Advanced Materials

ADVANCED MATERIALS
www.advmat.de

RESEARCH ARTICLE

Ambipolar Fiber Amplifiers for Highly Sensitive Biosignal Detection

Xin Zhang[1] | Siqi Fang[1,2] | Xiran Pan[1] | Yiheng Chen[1] | Wenxi Sun[1] | Zhanyu Qian[1] | Yuting Zheng[1] | Shahao Li[1] | Zhibo Ren[1] | Simin Liang[1] | Chuntao Lan[3] | Ting Lei[1] | Zhi Zhang[1]

[1]State Key Laboratory of Advanced Waterproof Materials, Engineering Research Center of Ministry of Education for Adaptive Biomaterials and Medical Devices, School of Materials Science and Engineering, Peking University, Beijing, China | [2]Guangdong Provincial Key Laboratory of Functional and Intelligent Hybrid Materials and Devices, South China Advanced Institute for Soft Matter Science and Technology, School of Emergent Soft Matter, South China University of Technology, Guangzhou, China | [3]College of Textile and Garment, Nantong University, Nantong, China

Correspondence: Simin Liang (liangsimin@pku.edu.cn) | Ting Lei (tinglei@pku.edu.cn) | Zhi Zhang (zhizhang@pku.edu.cn)

Received: 22 July 2026 | **Revised:** 28 October 2026 | **Accepted:** 2 November 2026

Keywords: organic electrochemical transistor | conjugated polymer | ambipolar material | biosignal amplifier | cortisol sensing

ABSTRACT

Biological signals are inherently weak and susceptible to noise, making in situ signal amplification critical for high-fidelity sensing. Electronic fibers offer unique advantages for conformal and scalable biointegration; however, fiber amplifiers are seldom reported due to the lack of suitable semiconducting materials that combine balanced ambipolar transport, scalable fiber fabrication, and high device performance. Herein, we report the first single-component ambipolar fiber platform based on a newly designed polymer, P(gTDPP-TQ), which combines balanced p- and n-type transport, low-cost synthesis, and continuous fiber fabrication. Fiber processing enhances molecular ordering and charge transport, yielding record-high μC^* and $g_{m,norm}$ among reported semiconducting fibers, enabling high-performance fiber amplifiers with a high voltage gain of up to 150 V V^{-1} and low operating voltages down to 0.5 V. These fiber amplifiers enable high-fidelity electroencephalogram signal amplification over 20 times and sensitive cortisol sensing with a record-low detection limit of 3.7 fM. This work establishes a general ambipolar fiber platform for integrated bioelectronic amplification and sensing.

1 | Introduction

Biological signals provide direct and dynamic access to physiological states, serving as fundamental information carriers for monitoring and understanding biological systems [1, 2]. Reliable acquisition is therefore important for signal processing and in-depth understanding [3, 4]. However, many physiological signals, such as microvolt-level electrophysiological activities and low-concentration biochemical analytes, are inherently weak and highly susceptible to noise [5, 6]. Conventional downstream amplification and filtering often suffer from signal degradation and distortion. Consequently, in situ signal amplification at the device–tissue interface is essential for preserving signal fidelity and enabling accurate detection [7, 8].

Organic electrochemical transistors (OECTs) provide an effective platform for signal amplification due to their intrinsically high transconductance (g_m) [9–11], which arises from volumetric electrochemical doping in organic mixed ionic-electronic conductors (OMIECs) [12, 13]. Nevertheless, individual OECTs mainly function as current amplifiers and are insufficient for signal-processing tasks requiring voltage gain and logic functionality.

Xin Zhang, Siqi Fang, and Xiran Pan contributed equally to this work.

All rights reserved, including rights for text and data mining and training of artificial intelligence technologies or similar technologies.
© 2026 Wiley-VCH GmbH

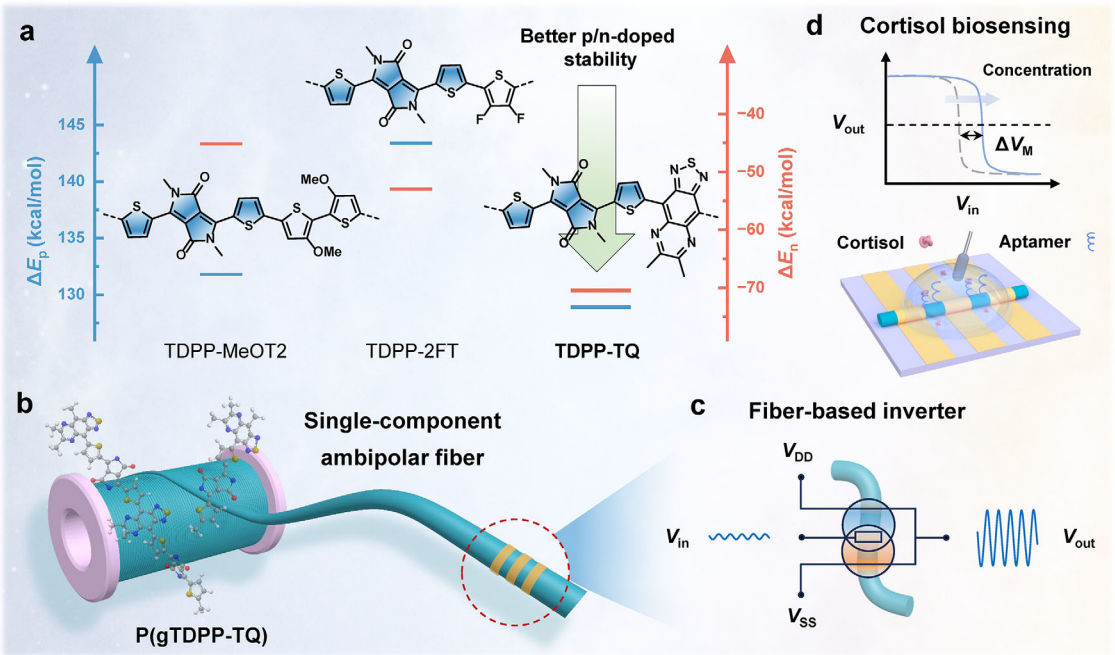


FIGURE 1 | Schematic illustration of the single-component ambipolar fiber amplifier platform. (a) Molecular design of P(gTDPP-TQ) polymer. (b) Continuous fabrication of single-component ambipolar fibers. Applications of the fiber amplifiers for (c) electrophysiological signal amplification and (d) cortisol biosensing.

Complementary p–n OECT inverters can enable voltage amplification with low static power consumption, yet their construction critically relies on integrating p- and n-type materials, which inevitably increases fabrication complexity and limits scalability [14, 15]. Ambipolar materials, capable of transporting both holes and electrons within a single component, offer a promising alternative by simplifying device architecture and facilitating integration and miniaturization. For practical implementation, such materials must balance high transport performance, operational stability, and scalable manufacturability [16–19]. However, most existing ambipolar materials suffer from unbalanced p/n performance, complicated molecular structures, and relatively high synthetic cost, limiting their practical applications in integrated bioelectronics [20–24]. Therefore, high-performance, cost-effective ambipolar materials are urgently needed to unlock their processing versatility and expand application scope.

Beyond material design, device geometry offers a powerful strategy for performance optimization. In this regard, fiber-based OECTs (F-OECTs) have emerged as a compelling architecture that enables continuous, scalable fabrication of volumetric devices through scalable processing [25, 26]. During spinning, directional flow and one-dimensional confinement can induce preferential molecular chain alignment and enhanced crystallinity in conjugated polymers [27, 28]. Such structural ordering not only facilitates more efficient charge transport and device performance, but the fiber geometry also provides mechanical compliance and compatibility with deformable biointerfaces [29–31]. To date, however, single-component ambipolar fibers have not been realized, largely due to intrinsic material limitations and high costs. Existing fiber inverters typically rely on integrating p- and n-type fibers, increasing manufacturing complexity and limiting device integration [32]. Blending p- and n-type materials into a single fiber offers an alternative, but transport mismatch typically degrades the figure-of-merit (μC^*) and voltage gain [33]. Consequently, ambipolar fibers and their applications fall far short of their potential.

In this work, we report a single-component ambipolar fiber and amplifiers based on a new polymer, P(gTDPP-TQ), which combines balanced p- and n-type charge transport, relatively simple and low-cost synthesis, and continuous wet-spinning capability (Figure 1a,b). This design overcomes the longstanding manufacturing complexity and charge-transport mismatch inherent in traditional multicomponent fiber amplifiers. Fiber processing enhances molecular ordering and OECT performance, yielding higher $g_{m,norm}$ and μC^* values than the thin-film counterpart for both p- and n-type operation. These high-performance fibers enable fiber amplifiers with a high voltage gain of up to 150 V V^{-1} (Figure 1c), enabling high-fidelity electroencephalogram (EEG) signal amplification exceeding 20-fold and sensitive cortisol sensing with a limit of detection (LOD) down to 3.7 fM (Figure 1d), surpassing previously reported cortisol sensors.

2 | Results and Discussion

2.1 | Rational Molecular Design, Synthesis, and Characterization

Achieving high-performance ambipolar OECT polymers typically relies on sophisticated proquinoidal building blocks, such as thienoisoindigo (TII) and thiophene-fused benzodifurandione-based oligo (*p*-phenylene vinylene) (TBDOPV), which effectively stabilize both p- and n-doped states, thereby enabling balanced ambipolar transport [24, 34]. However, these molecules generally

15214095, 0, Downloaded from https://advanced.onlinelibrary.wiley.com/doi/10.1002/adma.75671 by Zhi Zhang - Peking University , Wiley Online Library on [23/11/2026]. See the Terms and Conditions (https://onlinelibrary.wiley.com/terms-and-conditions) on Wiley Online Library for rules of use; OA articles are governed by the applicable Creative Commons License

require complicated multistep synthesis and limited scalability, which hinder their application in fiber bioelectronics. Therefore, developing structurally simple and low-cost ambipolar polymers with appropriate fiber spinnability, without compromising electrochemical performance, remains a key challenge.

To address this challenge, we designed P(gTDPP-TQ) using relatively simple and synthetically accessible building blocks. Commercially available 3,6-di(thiophen-2-yl)-2,5-dihydropyrrolo[3,4-c]pyrrole-1,4-dione (TDPP) was selected as the electron-deficient building block due to its simple structure, low cost, and highly planar backbone that facilitates efficient charge transport [35–38]. Meanwhile, 6,7-dimethyl-[1,2,5]thiadiazolo[3,4-g]quinoxaline (TQ) was introduced as another building block due to its strong proquinoidal feature and high hole/electron mobilities [39].

To rationally evaluate the electronic characteristics of this molecular design, density functional theory (DFT) calculations were conducted on P(gTDPP-TQ). Previous studies have shown that the doping characteristics of OECT polymers are highly dependent on the stability of their doped states, where electron-donating units (e.g., MeOT2) provided a p-type polymer while electron-withdrawing motifs (e.g., 2FT) led to n-type polymers [15]. The calculation results showed that introducing TQ unit effectively lowers the lowest unoccupied molecular orbital (LUMO) energy level while maintaining a high highest occupied molecular orbital (HOMO) energy level, suggesting its good potential for balanced ambipolar transport (Figure 1a). Moreover, the TDPP-TQ conjugated backbone exhibits a highly planar molecular geometry with a large torsional energy barrier (Figure S1), which is further enhanced upon doping. The reversible aromatic-quinoidal resonance transition enables the backbone to accommodate both hole and electron polarons (Figure 2b). Spin-density calculations further reveal that both polarons are highly delocalized along the conjugated backbone (Figure S2), suggesting favorable charge-carrier stabilization and ambipolar transport capability [34].

Based on the molecular design, P(gTDPP-TQ) was synthesized via Stille coupling between TDPP and TQ moieties (Figure 2a and Figures S3–S6). Ethylene glycol side chains were first grafted onto the TDPP unit to improve hydrophilicity and ion transport capability. Tris(butyl)tin was then introduced to the TDPP backbone for Stille polymerization using lithium diisopropylamide (LDA). Compared with previously reported ambipolar polymers that rely on complex fused-ring or highly elaborated proquinoidal structures, P(gTDPP-TQ) adopts a relatively simple and scalable molecular design with fewer synthetic steps and reduced cost (136 USD g^{-1}, Figure S7), highlighting its potential for large-scale preparation. The polymer exhibits a molecular weight of M_w/M_n = 44.1/17.9 kDa, with good thermal stability (Figure S8).

P(gTDPP-TQ) exhibited a characteristic low-energy absorption band associated with intramolecular charge transfer (Figure 2c). Compared with its dilute hexafluoroisopropanol (HFIP) solution, the absorption maximum of the polymer film exhibited a blue shift, probably due to stabilization of the excited charge-transfer state by the highly polar HFIP solvent. Cyclic voltammetry (CV) measurements revealed the HOMO/LUMO levels of −4.91/−4.22 eV, respectively (Figure 2d), corresponding to a narrow bandgap of 0.69 eV, facilitating both hole and electron injection. Spectroelectrochemical analysis was further performed to investigate the ambipolar doping capability. Upon increasing the bias voltage, the neutral-state absorption bands gradually diminished, accompanied by the emergence of polaron/bipolaron absorption bands at longer wavelengths under both oxidation and reduction with similar intensity (Figure 2e,f), suggesting that P(gTDPP-TQ) can efficiently generate and stabilize both positive and negative polarons.

2.2 | Balanced Ambipolar Charge Transport and OECT Properties

To validate whether the molecular design translates into balanced ambipolar transport, P(gTDPP-TQ) was first evaluated in film-based OECTs fabricated using our previously reported photolithography and parylene-patterning method [15]. Device performance was assessed based on Bernards' model [40]:

$$\mu C^* = \frac{g_m L}{Wd(V_G - V_{th})} \quad (1)$$

$$g_{m,norm} = \frac{g_m}{\frac{Wd}{L}} \quad (2)$$

where μC^* is the figure-of-merit. μ and C^* are the charge carrier mobility and the channel capacitance per unit volume, respectively; g_m is the transconductance in the saturation regime, and $g_{m,norm}$ is the normalized g_m used for fair comparison across devices of various sizes; W, L, and d are the channel width, length, and thickness, respectively; V_G and V_{th} are the applied gate voltage and threshold voltage, respectively.

P(gTDPP-TQ) film-based OECTs presented typical ambipolar characteristics with a balanced μC^* values of 50 ± 6 F cm^{-1} V^{-1} s^{-1} (p-type)/51 ± 6 F cm^{-1} V^{-1} s^{-1} (n-type) and $g_{m,norm}$ values of 10.2 ± 1.2 S cm^{-1} (p-type)/15.8 ± 1.8 S cm^{-1} (n-type) (Figure 3a,b and Table S1). The balanced hole and electron transport characteristics validate the molecular design strategy, demonstrating that incorporating the proquinoidal TQ unit effectively balances both p- and n-type electrochemical doping within a simple polymer backbone. Moreover, operational stability was evaluated under cyclic gate-voltage pulsing. The P(gTDPP-TQ) film-based OECTs exhibited good operational stability with negligible decay in on-currents over 200 switching cycles (Figure S9).

Benefiting from efficient volumetric ion transport, the P(gTDPP-TQ) film-based OECTs displayed fast response times (p-type: τ_{on}/τ_{off} = 0.34/0.04 ms; n-type: τ_{on}/τ_{off} = 0.33/0.04 ms). These values are among the shortest switching times reported for ambipolar OECTs (Figure 3c,d and Table S2), highlighting the efficient coupling between ionic and electronic transport in the P(gTDPP-TQ) channel.

The balanced ambipolar transport and rapid electrochemical switching further translated into good circuit performance. The ambipolar inverter based on a single P(gTDPP-TQ) film achieved an ultrahigh voltage gain of 907 V V^{-1} at V_{DD} = 0.8 V, outperforming previously reported ambipolar OECT inverters under comparable operating conditions (Figure 3e,f and Table S3).

15214095, 0, Downloaded from https://advanced.onlinelibrary.wiley.com/doi/10.1002/adma.75671 by Zhi Zhang - Peking University , Wiley Online Library on [23/11/2026]. See the Terms and Conditions (https://onlinelibrary.wiley.com/terms-and-conditions) on Wiley Online Library for rules of use; OA articles are governed by the applicable Creative Commons License

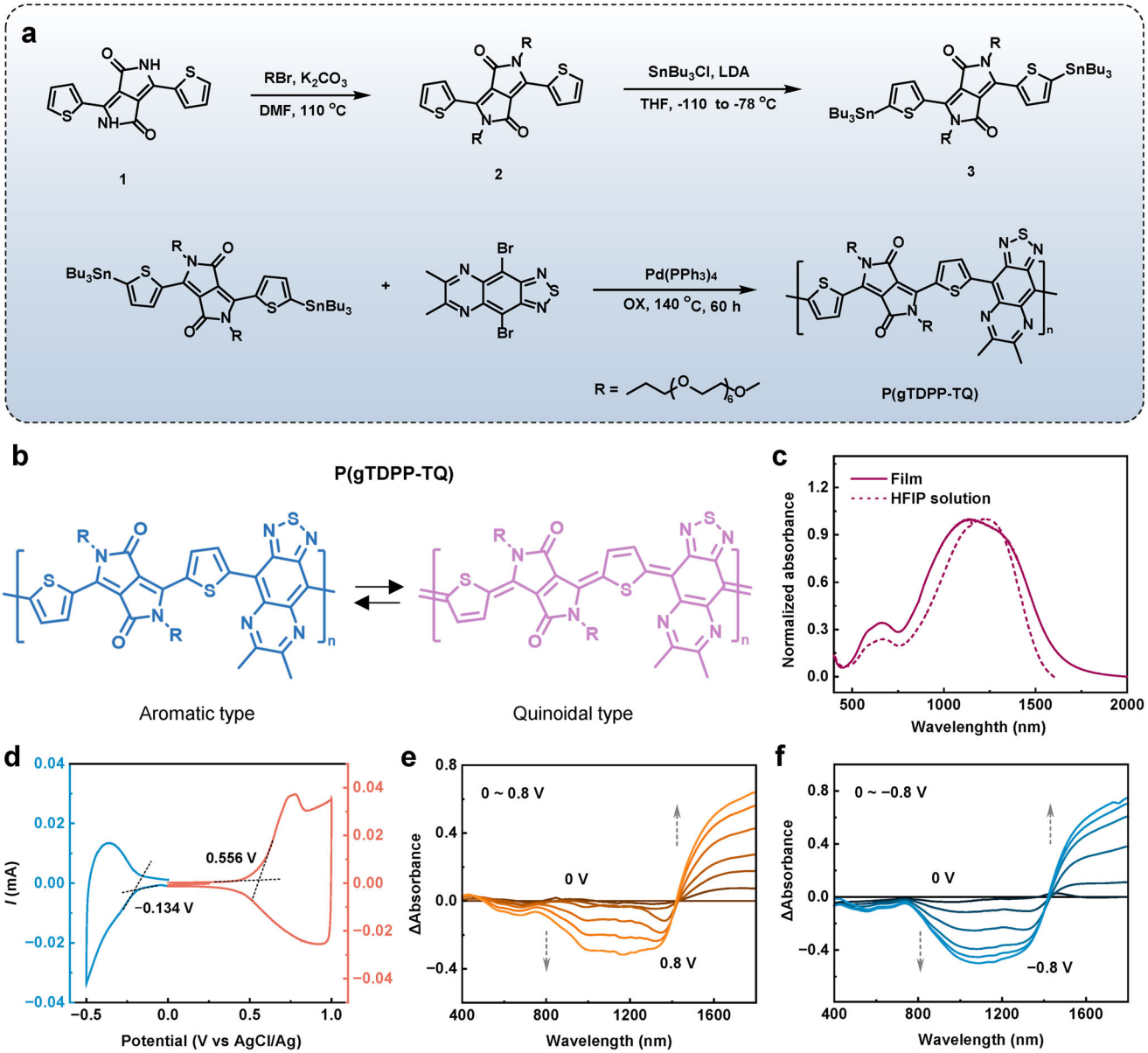


FIGURE 2 | (a) Synthetic route to P(gTDPP-TQ). (b) Aromatic and quinoidal structures of P(gTDPP-TQ). (c) Normalized absorption spectra of P(gTDPP-TQ) in film state and in HFIP solution. (d) CV curves of P(gTDPP-TQ) with Fc/Fc$^+$ as the external standard. Electrochemical absorption spectra of P(gTDPP-TQ) with (e) positive voltages (0 to 0.8 V) and (f) negative voltages (0 to −0.8 V) on ITO glass in 0.1 M NaCl aqueous solution. The absorbance represents the difference in absorption intensity at various bias voltages.

To elucidate the structural origin of the excellent device performance, grazing incidence wide-angle x-ray scattering (GIWAXS) was performed. The pristine P(gTDPP-TQ) film exhibited a mixed molecular packing orientation with a face-on dominant, featuring a lamellar distance (d_{lam}) of 25.7 Å and a π–π stacking distance ($d_{\pi-\pi}$) of 3.64 Å (Figure 3g and Table S4). Notably, upon exposure to 0.1 M NaCl, the P(gTDPP-TQ) film gradually evolved from a mixed molecular packing to a predominantly edge-on orientation, accompanied by reduced lamellar and π–π stacking distances of 23.8 and 3.62 Å, respectively. Meanwhile, increased coherence lengths ($L_{c,lam}$ and $L_{c,\pi-\pi}$) and reduced paracrystalline disorder parameters (g_{lam} and $g_{\pi-\pi}$) indicated a more compact and highly ordered molecular packing. Importantly, this ordered packing remained essentially unchanged throughout both the reduction and oxidation processes, demonstrating the exceptional structural stability of P(gTDPP-TQ) during electrochemical doping in 0.1 M NaCl and suggesting highly stable doped states (Figure 3h and Figure S10). Atomic Force Microscopy (AFM) further revealed a smooth and uniform film surface with a root-mean-square (RMS) roughness value of 0.78 nm (Figure 3i), indicating good film quality for stable OECT operation.

2.3 | Fiber Amplifiers for Biosignal Monitoring

Unlike spin-coated films, the fiber fabrication imposes stringent requirements on polymer chain rigidity, solubility, aggregation behavior, and overall processability, making the realization of high-performance ambipolar fibers particularly challenging. Previously reported ambipolar polymers, such as P(TII-2FT) and

15214095, 0, Downloaded from https://advanced.onlinelibrary.wiley.com/doi/10.1002/adma.75671 by Zhi Zhang - Peking University , Wiley Online Library on [23/11/2026]. See the Terms and Conditions (https://onlinelibrary.wiley.com/terms-and-conditions) on Wiley Online Library for rules of use; OA articles are governed by the applicable Creative Commons License

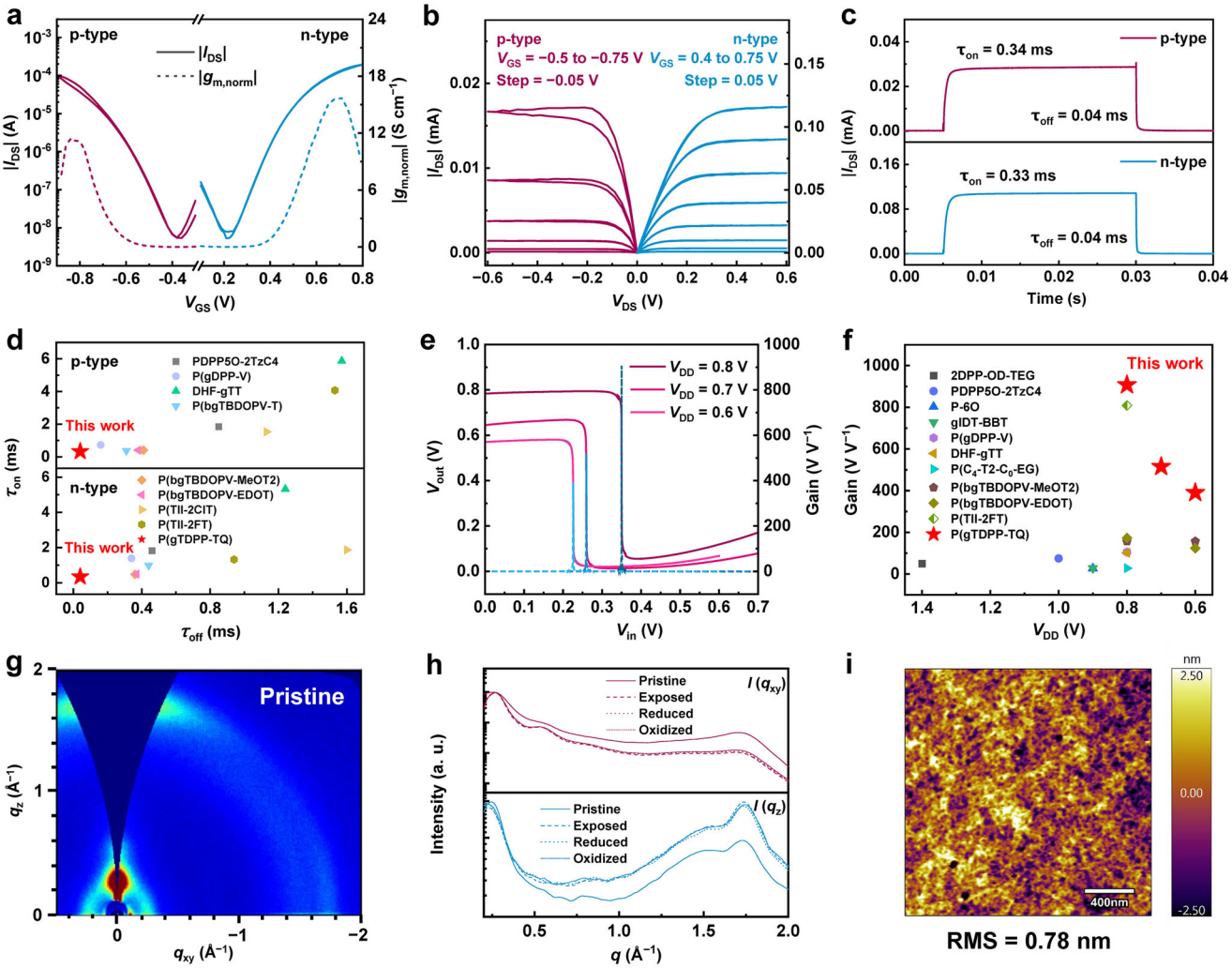


FIGURE 3 | (a) Transfer and (b) output characteristics of the OECT based on P(gTDPP-TQ). (c) Transient switching characteristics of the P(gTDPP-TQ) film-based OECT. On-state V_{GS} is the voltage at the maximum g_m, while the off-state V_{GS} is the voltage at the lowest current. (d) Comparison of τ_{on} and τ_{off} values of the P(gTDPP-TQ) film-based OECT with previously reported ambipolar OECTs [22, 24, 34, 38, 41]. (e) Voltage transfer characteristics and gains of the P(gTDPP-TQ) film-based inverter at different V_{DD}. (f) Gain values of reported ambipolar OECT-based inverters at different V_{DD} [21, 22, 24, 34, 38, 41–44]. (g) 2D-GIWAXS pattern of the pristine P(gTDPP-TQ) film. (h) Line-cut profiles of the GIWAXS patterns for P(gTDPP-TQ) films under pristine, exposed, reduced, and oxidized states. (i) AFM height image of the P(gTDPP-TQ) film.

P(bgTBDOPV-EDOT), fail to satisfy these processing requirements. For example, the limited intermolecular interactions and insufficient chain entanglement of P(TII-2FT) hinder the formation of mechanically robust filaments, whereas the highly fused and structurally complex backbone of P(bgTBDOPV-EDOT) leads to poor processability and high synthetic complexity. These limitations are commonly observed across existing ambipolar systems. These limitations highlight the challenge of developing ambipolar polymers that simultaneously satisfy electrochemical performance and fiber processability requirements.

P(gTDPP-TQ) is specifically designed to balance solution processability, aggregation behavior, and electronic functionality, enabling stable fiber formation using our previously reported "FLEX" wet-spinning method [45]. In contrast to previously discussed ambipolar polymers, P(gTDPP-TQ) features a simple molecular structure that enables low-cost synthesis, while simultaneously achieving an optimal balance between solubility and interchain interactions. By carefully designing solvent-polymer interactions and coagulation dynamics, continuous P(gTDPP-TQ) fibers were successfully produced. Specifically, trifluoroethanol (TFE) was selected as the spinning solvent because it maintains high polymer dispersibility while promoting stronger interchain aggregation than HFIP and providing good solution stability (Figures S11–S13). This balance facilitates chain interaction during solvent exchange and supports continuous fiber formation. The coagulation bath was further screened to regulate chain assembly during solvent exchange (Figures S14 and S15). The as-prepared P(gTDPP-TQ) fibers featured a smooth surface, uniform diameter, and favorable mechanical strength (Figure 4a and Figure S16).

To understand the structural evolution induced by fiber processing, both high-resolution transmission electron microscopy (HRTEM) and wide-angle X-ray scattering (WAXS) analyses were performed. HRTEM revealed a clear crystal lattice in both the

15214095, 0, Downloaded from https://advanced.onlinelibrary.wiley.com/doi/10.1002/adma.75671 by Zhi Zhang - Peking University , Wiley Online Library on [23/11/2026]. See the Terms and Conditions (https://onlinelibrary.wiley.com/terms-and-conditions) on Wiley Online Library for rules of use; OA articles are governed by the applicable Creative Commons License

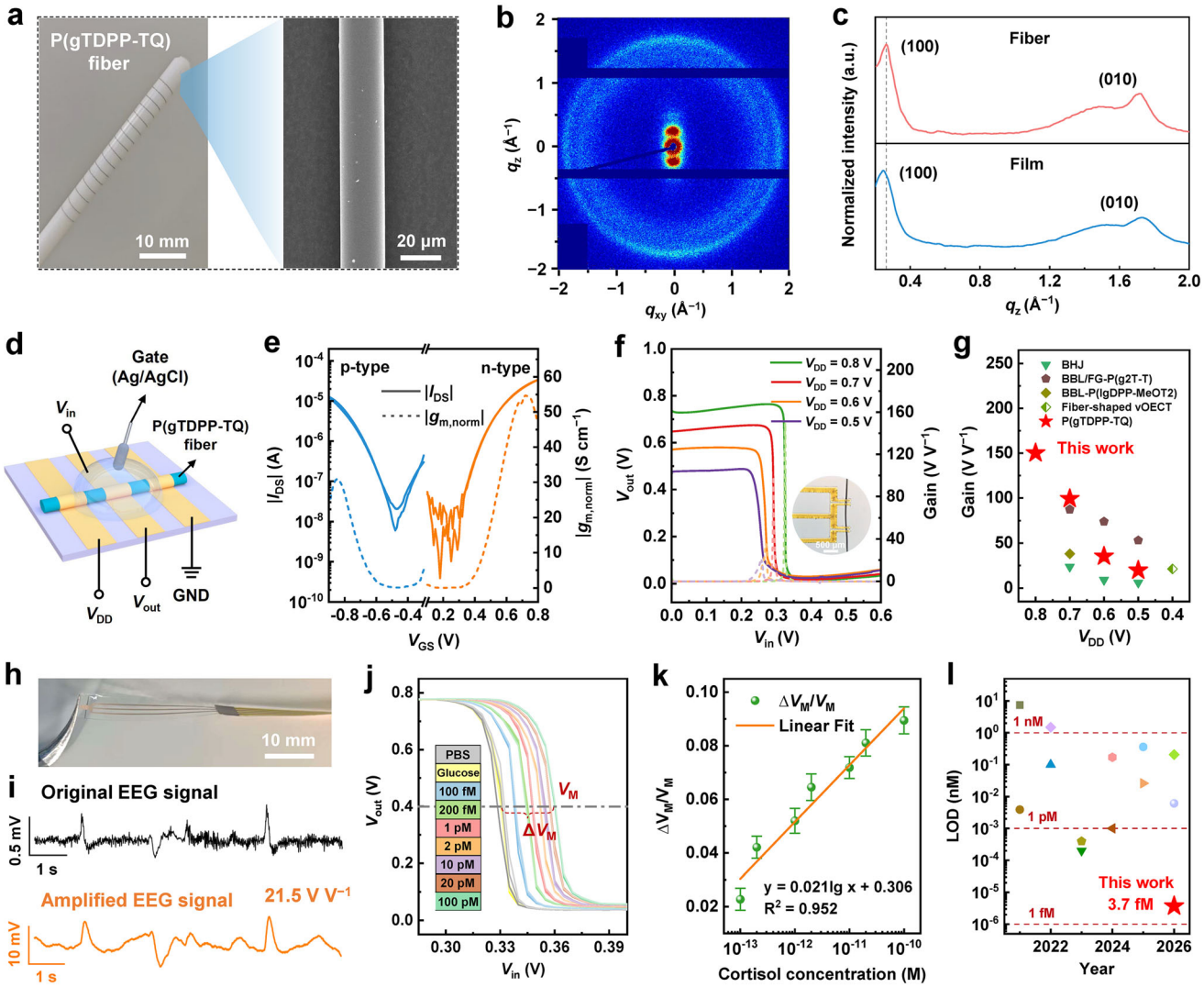


FIGURE 4 | (a) Optical photograph (left) and scanning electron microscopy (SEM) image (right) of the P(gTDPP-TQ) fiber. (b) 2D-WAXS pattern of the P(gTDPP-TQ) fiber. (c) Line-cut profiles of the WAXS/GIWAXS pattern for P(gTDPP-TQ) fiber and P(gTDPP-TQ) film. (d) Schematic illustration of the device configuration of the P(gTDPP-TQ) F-OECT and fiber inverter. (e) Transfer characteristics of the P(gTDPP-TQ) F-OECT. (f) Voltage transfer characteristics and gains of the P(gTDPP-TQ) fiber inverter. (g) Comparison of gain values of the P(gTDPP-TQ) fiber-based amplifier with reported fiber amplifiers at various V_{DD} [32, 33, 49, 50]. (h) Photograph of the P(gTDPP-TQ) fiber inverter integrated on a poly(styrene-b-(ethylene-co-butylene)-b-styrene) (SEBS) flexible substrate and (i) the amplified EEG signal recorded using the fiber amplifier. (j) Voltage transfer characteristics of the cortisol sensor with aptamer-functionalized channels exposed to phosphate-buffered saline (PBS), glucose, and different concentrations of cortisol solutions. (k) Normalized response curves derived from the switching voltage shift of the cortisol sensor. (l) Comparison of LOD of the P(gTDPP-TQ) fiber inverter-based cortisol sensor with previously reported sensors [51–62].

P(gTDPP-TQ) film and fiber, with comparable π–π stacking distances of approximately 0.36 nm (Figure S17), indicating that good molecular packing is preserved during fiber processing. WAXS measurements further showed that, compared with the spin-coated film, P(gTDPP-TQ) fibers exhibited enhanced orientation and distinctly reduced paracrystalline disorder (*g* factor), and more compact packing with a decreased lamellar distance of 24.9 Å (Figure 4b,c and Table S5). These correlated structural changes are all expected to facilitate charge transport by improving molecular ordering and reducing structural disorder. Among them, the pronounced molecular orientation induced by fiber spinning is likely an important contributor. Flow-induced shear has been reported to promote conjugated polymer ordering and charge transport [46, 47], and the directional flow field during fiber spinning can further enhance long-range molecular alignment, providing a favorable structural basis for high-performance F-OECTs [48, 49].

Capitalizing on the inherent ambipolar characteristics of P(gTDPP-TQ), a single P(gTDPP-TQ) fiber was directly employed as the channel material to construct the F-OECTs and inverter-based amplifiers with simplified device architecture (Figure 4d). This represents a major simplification over conventional fiber inverters that rely on the physical integration of distinct p- and n-type components [32, 33, 49, 50]. The resulting F-OECTs delivered excellent ambipolar performance, achieving enhanced μC^* values of 136 ± 18 F cm^{-1} V^{-1} s^{-1} (p-type)/141 ± 15 F cm^{-1} V^{-1} s^{-1} (n-type) and high $g_{m,norm}$ values of 33.1 ± 4.7 S cm^{-1}

15214095, 0, Downloaded from https://advanced.onlinelibrary.wiley.com/doi/10.1002/adma.75671 by Zhi Zhang - Peking University , Wiley Online Library on [23/11/2026]. See the Terms and Conditions (https://onlinelibrary.wiley.com/terms-and-conditions) on Wiley Online Library for rules of use; OA articles are governed by the applicable Creative Commons License

(p-type)/46.1 ± 5.4 S cm^{-1} (n-type) (Table S6). Notably, these $g_{m,norm}$ values outperform those of the film counterparts as well as previously reported ambipolar OECTs based on both film and fiber architectures (Figures 4e and S18; Tables S7 and S8). The enhanced F-OECT performance likely arises from the combined effects of improved molecular orientation, reduced structural disorder, and more compact packing induced by fiber processing. The P(gTDPP-TQ) F-OECTs also maintained favorable operational stability (Figure S19). The corresponding fiber inverter exhibited excellent voltage amplification capability with a sharp switching transition and a high voltage gain of 150 V V^{-1} at V_{DD} = 0.8 V (Figure 4f). Notably, the μC^*, $g_{m,norm}$, and gain values significantly outperform those of state-of-the-art fiber inverters based on two-component architectures (Figure 4g and Table S8), demonstrating that balanced ambipolar transport in a single-component fiber can effectively translate into superior device performance.

Fiber architecture holds great promise for biointerface and wearable biosignal monitoring applications, where long-term and intimate contact with biological tissues is required. The biocompatibility of P(gTDPP-TQ) fibers was evaluated by cell viability assays. All mouse fibroblasts (NIH/3T3) cultured on the P(gTDPP-TQ) fiber remained fully alive (green fluorescence) with no obvious cytotoxic effects observed (Figure S20). These results demonstrate the good biocompatibility of P(gTDPP-TQ) fibers and support their potential for integration into long-term wearable and implantable bioelectronic systems.

Beyond demonstrating excellent device performance, the flexible fiber-based inverter was further explored as a universal platform for multimodal biosignal amplification, including electrical and biochemical signals. Electrophysiological signals, such as EEG, typically exhibit low amplitudes and require signal amplification for high-fidelity acquisition. The P(gTDPP-TQ) fiber inverter was therefore used as a voltage amplifier for simulated EEG monitoring. The recorded EEG signal was successfully amplified by a factor of 21.5, while preserving the original signal characteristics, demonstrating the capability of the fiber-based circuit for high-fidelity amplification of weak bioelectrical signals (Figure 4h,i).

The versatility of this fiber-based amplification platform was further extended to biochemical sensing. Cortisol, a key biomarker of stress and physiological homeostasis which plays a critical role in health monitoring and early disease intervention, was selected as a model analyte. To enable selective cortisol recognition, the surface of the P(gTDPP-TQ) fiber channel was functionalized with amino-modified cortisol aptamers through carbodiimide coupling chemistry, allowing specific binding events to modulate the interfacial electrochemical environment of the OECT channel.

Upon cortisol exposure, the voltage transfer curves of the fiber inverter exhibited a systematic rightward shift with increasing cortisol concentration (Figure 4j), indicating effective modulation of the inverter switching behavior. The switching voltage (V_M), defined as the input voltage (V_{in}) corresponding to half of the supply voltage (1/2 V_{DD} = 0.4 V), was extracted as the sensing signal. Compared with conventional electrochemical sensors that typically rely on direct current readout, the inverter configuration enables intrinsic signal amplification by converting molecular recognition events into amplified voltage outputs. Highly reproducible responses were obtained over repeated measurements, demonstrating excellent operational stability. The switching voltage shift (ΔV_M) exhibited a strong linear dependence on cortisol concentration over a wide range from 100 fM to 100 pM (R^2 > 0.95) (Figure 4k), with an ultralow LOD of 3.7 fM at a signal-to-noise ratio (SNR) of 3. This performance ranks among the best reported performances for cortisol sensors (Figure 4l and Table S9). Furthermore, a negligible response was observed in the presence of 10 μM glucose, demonstrating excellent selectivity of the fiber-based cortisol sensor. These results demonstrate that the P(gTDPP-TQ) fiber inverter serves not only as an amplification circuit but also as a versatile bioelectronic transduction platform capable of converting biochemical recognition events into amplified electrical signals.

3 | Conclusions

In summary, we have established a single-component ambipolar polymer fiber platform that overcomes the longstanding trade-offs between material cost, charge-transport balance, and processing scalability in fibrous ambipolar OECTs. We demonstrate that P(gTDPP-TQ) is easily compatible with wet-spinning processing, where the spinning process synergistically induces enhanced molecular alignment, reduced structural disorder, and charge transport, yielding the first single-component ambipolar polymer fibers. The resulting F-OECTs deliver benchmark ambipolar performance among ambipolar fibers, with high μC^*, $g_{m,norm}$, and voltage gains of up to 150 V V^{-1}. These fiber amplifiers further enable >20-fold EEG signal amplification and cortisol sensing with a detection limit of 3.7 fM. We envision that the cost-effectiveness, scalable processability, and mechanical compliance of P(gTDPP-TQ) fibers will facilitate the development of next-generation intelligent textiles for continuous, high-fidelity, real-time monitoring of neurological and endocrine activities.

Author Contributions

T.L. and Z.Z. conceptualized and supervised the project. X.P., Shahao L., and Z.R. synthesized the polymers. X.Z., S.F., X.P., Simin L., Y.C., W.S., Z.Q., and Y.Z. performed the experiments and characterizations. X.P. conducted the DFT calculations. X.Z., S.F., X.P., Simin L., C.L., T.L., and Z.Z. analyzed the experimental data and wrote the manuscript. All the authors revised and approved the manuscript.

Acknowledgements

We acknowledge the financial support from National Key R&D Program of China (2025YFF0518302), National Natural Science Foundation of China (T2425010, T2521001, and 5243219), Beijing Natural Science Foundation (2262050) and the Fundamental Research Funds for the Central Universities, Peking University (PKU2026PKULCXQ023). We acknowledge the Electron Microscopy Laboratory, the Materials Processing and Analysis Center, and the Molecular Materials and Nanofabrication Laboratory (MMNL) at Peking University for granting access to their instruments. We thank Optical Imaging Core Facility, National Center for Protein Sciences at Peking University in Beijing, China, for assistance with data acquisition. Computational resources were provided by the High-Performance Computing Platform at Peking University.

15214095, 0, Downloaded from https://advanced.onlinelibrary.wiley.com/doi/10.1002/adma.75671 by Zhi Zhang - Peking University , Wiley Online Library on [23/11/2026]. See the Terms and Conditions (https://onlinelibrary.wiley.com/terms-and-conditions) on Wiley Online Library for rules of use; OA articles are governed by the applicable Creative Commons License

Conflicts of Interest

The authors declare no conflicts of interest.

Data Availability Statement

The data that support the findings of this study are available from the corresponding author upon reasonable request.

References

1. C. Z. Zhao, J. Park, S. E. Root, and Z. N. Bao, "Skin-Inspired Soft Bioelectronic Materials, Devices and Systems," *Nature Reviews Bioengineering* 2 (2024): 671–690, https://doi.org/10.1038/s44222-024-00194-1.

2. H. J. Kim, J. H. Koo, S. Lee, T. Hyeon, and D. H. Kim, "Materials Design and Integration Strategies for Soft Bioelectronics in Digital Healthcare," *Nature Reviews Materials* 10 (2025): 654–673, https://doi.org/10.1038/s41578-025-00819-w.

3. J. Y. Yin, S. L. Wang, T. Tat, and J. Chen, "Motion Artefact Management for Soft Bioelectronics," *Nature Reviews Bioengineering* 2 (2024): 541–558, https://doi.org/10.1038/s44222-024-00175-4.

4. P. D. Fan, Y. Liu, Y. X. Pan, Y. B. Ying, and J. F. Ping, "Three-Dimensional Micro- and Nanomanufacturing Techniques for High-Fidelity Wearable Bioelectronics," *Nature Reviews Electrical Engineering* 2 (2025): 390–406, https://doi.org/10.1038/s44287-025-00174-6.

5. S.-H. Sunwoo, S. I. Han, C. S. Park, et al., "Soft Bioelectronics for the Management of Cardiovascular Diseases," *Nature Reviews Bioengineering* 2 (2023): 8–24, https://doi.org/10.1038/s44222-023-00102-z.

6. N. Brasier, J. Wang, W. Gao, et al., "Applied Body-Fluid Analysis by Wearable Devices," *Nature* 636 (2024): 57–68, https://doi.org/10.1038/s41586-024-08249-4.

7. P. Y. Li, W. X. Sun, J. L. Li, et al., "N-Type Semiconducting Hydrogel," *Science* 384 (2024): 557–563, https://doi.org/10.1126/science.adj4397.

8. J. Zhang, Z. Cheng, P. J. Li, and B. Z. Tian, "Materials and Device Strategies to Enhance Spatiotemporal Resolution in Bioelectronics," *Nature Reviews Materials* 10 (2025): 425–448, https://doi.org/10.1038/s41578-025-00798-y.

9. J. Rivnay, S. Inal, A. Salleo, R. M. Owens, M. Berggren, and G. G. Malliaras, "Organic Electrochemical Transistors," *Nature Reviews Materials* 3 (2018): 17086, https://doi.org/10.1038/natrevmats.2017.86.

10. W. Huang, J. H. Chen, Y. Yao, et al., "Vertical Organic Electrochemical Transistors for Complementary Circuits," *Nature* 613 (2023): 496–502, https://doi.org/10.1038/s41586-022-05592-2.

11. P. Y. Li and T. Lei, "Toward Ideal Biointerfacing Electronics Using Organic Electrochemical Transistors," *Accounts of Materials Research* 6 (2025): 853–864, https://doi.org/10.1021/accountsmr.5c00030.

12. B. D. Paulsen, K. Tybrandt, E. Stavrinidou, and J. Rivnay, "Organic Mixed Ionic–Electronic Conductors," *Nature Materials* 19 (2020): 13–26, https://doi.org/10.1038/s41563-019-0435-z.

13. Y. Z. Wang, S. Wustoni, J. Surgailis, Y. Z. Zhong, A. Koklu, and S. Inal, "Designing Organic Mixed Conductors for Electrochemical Transistor Applications," *Nature Reviews Materials* 9 (2024): 249–265, https://doi.org/10.1038/s41578-024-00652-7.

14. P. Romele, P. Gkoupidenis, D. A. Koutsouras, et al., "Multiscale Real Time and High Sensitivity Ion Detection With Complementary Organic Electrochemical Transistors Amplifier," *Nature Communications* 11 (2020): 3743, https://doi.org/10.1038/s41467-020-17547-0.

15. P. Y. Li, J. W. Shi, Y. Q. Lei, Z. Huang, and T. Lei, "Switching P-Type to High-Performance N-Type Organic Electrochemical Transistors via Doped State Engineering," *Nature Communications* 13 (2022): 5970, https://doi.org/10.1038/s41467-022-33553-w.

16. V. N. Le, K. N. Baustert, M. R. Brown, et al., "Improved Organic Electrochemical Transistor Stability Using Solvent Degassing and Chemical Doping," *Nature Electronics* 8 (2025): 116–126, https://doi.org/10.1038/s41928-024-01297-8.

17. Z. F. Yao, J. Y. Wang, and J. Pei, "Side Chain Engineering Toward Chemical Doping of Conjugated Polymers," *Accounts of Chemical Research* 58 (2025): 1496–1508, https://doi.org/10.1021/acs.accounts.5c00121.

18. J.-L. Li, X.-Y. Deng, J. P. Chen, et al., "Cationic Conjugated Polymers With Enhanced Doped-State Planarity for N-Type Organic Thermoelectrics," *CCS Chemistry* 7 (2025): 1449–1458, https://doi.org/10.31635/ccschem.024.202404274.

19. T. C. Hidalgo Castillo, J. F. Ponder, K. Feng, et al., "Side Chains Override Crystallinity in n-Type Organic Mixed Conductors," *Advanced Materials* 38 (2026): e21048, https://doi.org/10.1002/adma.202521048.

20. X. H. Wu, T. L. D. Tam, S. Chen, et al., "All-Polymer Bulk-Heterojunction Organic Electrochemical Transistors With Balanced Ionic and Electronic Transport," *Advanced Materials* 34 (2022): 2206118, https://doi.org/10.1002/adma.202206118.

21. Y. M. Sun, Y. Lan, M. S. Li, et al., "Indacenodithiophene-Based Single-Component Ambipolar Polymer for High-Performance Vertical Organic Electrochemical Transistors and Inverters," *Aggregate* 5 (2024): e577, https://doi.org/10.1002/agt2.577.

22. G. Y. Qi, M. N. Wang, S. J. Wang, et al., "High-Performance, Single-Component Ambipolar Organic Electrochemical Transistors With Balanced N/P-Type Properties for Inverter and Biosensor Applications," *Advanced Functional Materials* 35 (2024): 2413112, https://doi.org/10.1002/adfm.202413112.

23. X. Q. Wang, C. Song, and T. Lei, "Open-Shell Oligomers and Polymers: Theory, Characterization Methods, Molecular Design, and Applications," *Chinese Journal of Polymer Science* 42 (2024): 417–436, https://doi.org/10.1007/s10118-024-3087-7.

24. G.-Y. Ge, J. C. Xu, X. Y. Wang, et al., "On-Site Biosignal Amplification Using a Single High-Spin Conjugated Polymer," *Nature Communications* 16 (2025): 396, https://doi.org/10.1038/s41467-024-55369-6.

25. Y. Y. Huang, Z. J. Hu, S. W. Zhu, and B. Fang, "Fibre-Based Organic Electrochemical Transistors: Principle, Evaluation, and Application," *NPJ Flexible Electronics* 9 (2025): 43, https://doi.org/10.1038/s41528-025-00417-4.

26. Y. Shin, Y. J. Jo, Y.-S. Ye, et al., "Fiber-Based Organic Electrochemical Transistors for Re-Shaping Bioelectronics: Integration on and in Textiles," *NPJ Flexible Electronics* 9 (2025): 112, https://doi.org/10.1038/s41528-025-00488-3.

27. J. Y. Feng, Y. Fang, C. Wang, et al., "All-Polymer Fiber Organic Electrochemical Transistor for Chronic Chemical Detection in the Brain," *Advanced Functional Materials* 33 (2023): 2214945, https://doi.org/10.1002/adfm.202214945.

28. S. L. Zhang, L. Chen, P. N. Chen, et al., "Technology Roadmap From Fiber Materials to Fiber Electronics," *National Science Review* 13 (2026): nwag368, https://doi.org/10.1093/nsr/nwag368.

29. C. Q. Tang, S. H. Yu, W. J. Li, et al., "Design, Construction, and Application of Implantable Fiber Biosensors," *Advanced Materials* 38 (2026): e08190, https://doi.org/10.1002/adma.202508190.

30. H. Kim, H. Y. Kim, J. H. Koo, G. D. Cha, D. H. Kim, and H. J. Kim, "Fiber-Type Soft Bioelectronics for Wearable and Implantable Sensing and Therapy," *BMEMat* 4 (2026): e70043, https://doi.org/10.1002/bmm2.70043.

31. M. Y. Xu, Z. W. Lin, X. L. Tong, D. Z. Yang, and Y. L. Shao, "Biomaterial-Based Fibrous Implantable Probes for Tissue-Electronics Interface," *Advanced Materials* 37 (2025): 2504372, https://doi.org/10.1002/adma.202504372.

32. X. Y. Wang, H. Jiang, H. Y. Wang, et al., "Shear-Intensified Hybridization of Conjugated Polymer Fibers for Organic Electrochemical Transistors," *Advanced Functional Materials* 36 (2025): e15197, https://doi.org/10.1002/adfm.202515197.

15214095, 0, Downloaded from https://advanced.onlinelibrary.wiley.com/doi/10.1002/adma.75671 by Zhi Zhang - Peking University , Wiley Online Library on [23/11/2026]. See the Terms and Conditions (https://onlinelibrary.wiley.com/terms-and-conditions) on Wiley Online Library for rules of use; OA articles are governed by the applicable Creative Commons License

33. H. Jiang, C.-Y. Yang, C. Y. Du, et al., "Ambipolar Bulk Heterojunction Semiconductor Fibers for High-Performance Neuromorphic Systems," *ACS Nano* 20 (2026): 11652–11661, https://doi.org/10.1021/acsnano.5c19192.

34. X. R. Pan, Z. B. Ren, Y. H. Chen, et al., "Strong Proquinoidal Acceptor Enables High-Performance Ambipolar Organic Electrochemical Transistors," *Advanced Materials* 37 (2025): 2417146, https://doi.org/10.1002/adma.202417146.

35. Y. Q. Lei, P. Y. Li, Y. T. Zheng, and T. Lei, "Materials Design and Applications of N-Type and Ambipolar Organic Electrochemical Transistors," *Materials Chemistry Frontiers* 8 (2024): 133–158, https://doi.org/10.1039/d3qm00828b.

36. G. C. Zhu, Y. P. Lai, J. X. Pu, J. H. Chen, and L. W. Feng, "Selenophene π -Bridge Enables Balanced Ambipolar Transport in High-Performance Organic Electrochemical Transistors," *Advanced Science* 13 (2026): e76016, https://doi.org/10.1002/advs.76016.

37. Y. M. Wang, J. T. Tan, H. Q. Hou, et al., "High Performing Ambipolar Organic Electrochemical Transistors and Solid-State Inverters Enabled by Hydrophilic/Hydrophobic Side Chains Integration," *Advanced Materials* 38 (2026): e15186, https://doi.org/10.1002/adma.202515186.

38. J. Z. Li, Z. Li, J. Y. Huang, et al., "High-Performance Ambipolar Organic Electrochemical Transistors Based on Diketopyrrolopyrrole-Dialkoxybithiazole Conjugated Polymers for Single-Component Inverters," *Advanced Science* 13 (2026): e20003, https://doi.org/10.1002/advs.202520003.

39. X.-X. Chen, J.-T. Li, Y.-H. Fang, et al., "High-Mobility Semiconducting Polymers With Different Spin Ground States," *Nature Communications* 13 (2022): 2258, https://doi.org/10.1038/s41467-022-29918-w.

40. D. A. Bernards and G. G. Malliaras, "Steady-State and Transient Behavior of Organic Electrochemical Transistors," *Advanced Functional Materials* 17 (2007): 3538–3544, https://doi.org/10.1002/adfm.200601239.

41. S. Y. Cong, J. X. Chen, M. Xie, et al., "Single Ambipolar OECT–Based Inverter With Volatility and Nonvolatility on Demand," *Science Advances* 10 (2024): eadq9405, https://doi.org/10.1126/sciadv.adq9405.

42. J. J. Samuel, A. Garudapalli, A. A. Mohapatra, C. Gangadharappa, S. Patil, and N. P. B. Aetukuri, "Single-Component CMOS-Like Logic Using Diketopyrrolopyrrole-Based Ambipolar Organic Electrochemical Transistors," *Advanced Functional Materials* 31 (2021): 2102903, https://doi.org/10.1002/adfm.202102903.

43. T. Pan, X. Jiang, E. R. W. van Doremaele, et al., "Over 60 h of Stable Water-Operation for N-Type Organic Electrochemical Transistors With Fast Response and Ambipolarity," *Advanced Science* 11 (2024): 2400872, https://doi.org/10.1002/advs.202400872.

44. R. B. Rashid, W. Y. Du, S. Griggs, I. P. Maria, I. McCulloch, and J. Rivnay, "Ambipolar Inverters Based on Cofacial Vertical Organic Electrochemical Transistor Pairs for Biosignal Amplification," *Science Advances* 7 (2021): eabh1055, https://doi.org/10.1126/sciadv.abh1055.

45. Z. Zhang, P. Y. Li, M. Xiong, et al., "Continuous Production of Ultratough Semiconducting Polymer Fibers With High Electronic Performance," *Science Advances* 10 (2024): eadk0647, https://doi.org/10.1126/sciadv.adk0647.

46. K. S. Park, J. J. Kwok, R. Dilmurat, et al., "Tuning Conformation, Assembly, and Charge Transport Properties of Conjugated Polymers by Printing Flow," *Science Advances* 5 (2019): eaaw7757, https://doi.org/10.1126/sciadv.aaw7757.

47. Y. C. Xu, Y. Y. Zhou, L. Ding, et al., "Tuning Solution-State Aggregation for Shearing-Induced Alignment and High Mobility Transport in Conjugated Polymers," *Advanced Materials* 38 (2026): e21831, https://doi.org/10.1002/adma.202521831.

48. H. Jiang, C.-Y. Yang, D. Y. Tu, et al., "Shear-Enhanced Liquid-Crystal Spinning of Conjugated Polymer Fibers," *National Science Review* 12 (2025): nwaf331, https://doi.org/10.1093/nsr/nwaf331.

49. X. Wang, Z. Zhang, P. Y. Li, et al., "Ultrastable N-Type Semiconducting Fiber Organic Electrochemical Transistors for Highly Sensitive Biosensors," *Advanced Materials* 36 (2024): 2400287, https://doi.org/10.1002/adma.202400287.

50. Y. H. Zhong, Q. C. Liang, Z. Chen, et al., "High-Performance Fiber-Shaped Vertical Organic Electrochemical Transistors Patterned by Surface Photolithography," *Chemistry of Materials* 35 (2023): 9739–9746, https://doi.org/10.1021/acs.chemmater.3c02237.

51. C. Cheng, X. Li, G. Xu, et al., "Battery-Free, Wireless, and Flexible Electrochemical Patch for In Situ Analysis of Sweat Cortisol via Near Field Communication," *Biosensors and Bioelectronics* 172 (2021): 112782, https://doi.org/10.1016/j.bios.2020.112782.

52. J. S. Nah, S. C. Barman, M. A. Zahed, et al., "A Wearable Microfluidics-Integrated Impedimetric Immunosensor Based on Ti3C2T MXene Incorporated Laser-Burned Graphene for Noninvasive Sweat Cortisol Detection," *Sensors and Actuators B: Chemical* 329 (2021): 129206, https://doi.org/10.1016/j.snb.2020.129206.

53. T. Laochai, J. Yukird, N. Promphet, J. Q. Qin, O. Chailapakul, and N. Rodthongkum, "Non-Invasive Electrochemical Immunosensor for Sweat Cortisol Based on L-Cys/Aunps/Mxene Modified Thread Electrode," *Biosensors and Bioelectronics* 203 (2022): 114039, https://doi.org/10.1016/j.bios.2022.114039.

54. S. Demuru, J. Kim, M. El Chazli, et al., "Antibody-Coated Wearable Organic Electrochemical Transistors for Cortisol Detection in Human Sweat," *ACS Sensors* 7 (2022): 2721–2731, https://doi.org/10.1021/acssensors.2c01250.

55. N. K. Singh, S. Chung, A. Y. Chang, J. Wang, and D. A. Hall, "A Non-Invasive Wearable Stress Patch for Real-Time Cortisol Monitoring Using a Pseudoknot-Assisted Aptamer," *Biosensors and Bioelectronics* 227 (2023): 115097, https://doi.org/10.1016/j.bios.2023.115097.

56. D. H. Lee, W. Y. Lee, and J. Kim, "Introducing Nanoscale Electrochemistry in Small-Molecule Detection for Tackling Existing Limitations of Affinity-Based Label-Free Biosensing Applications," *Journal of the American Chemical Society* 145 (2023): 17767–17778, https://doi.org/10.1021/jacs.3c04458.

57. L. Y. Jing, Y. K. Fan, B. Z. Chen, et al., "An Aptamer-Integrated Conductive Microneedle Biosensor for Real-Time Transdermal Cortisol Monitoring," *Chemical Engineering Journal* 502 (2024): 157488, https://doi.org/10.1016/j.cej.2024.157488.

58. X. K. Hu, Y. Y. Chen, X. Wang, et al., "Wearable and Regenerable Electrochemical Fabric Sensing System Based on Molecularly Imprinted Polymers for Real-Time Stress Management," *Advanced Functional Materials* 34 (2024): 2312897, https://doi.org/10.1002/adfm.202312897.

59. Y. Liu, X. Y. Su, P. D. Fan, X. Liu, Y. X. Pan, and J. F. Ping, "Computationally-Assisted Wearable System for Continuous Cortisol Monitoring," *Science Bulletin* 70 (2025): 2004–2013, https://doi.org/10.1016/j.scib.2025.03.060.

60. G. Dykstra, V. Vera, I. Chapa, S. Rao, and Y. X. Liu, "Engineering Electropolymerized Molecularly Imprinted Polymer Films for Redox-Integrated, Reagent-Free Cortisol Detection: The Critical Role of Scan Rate," *Biosensors and Bioelectronics* 286 (2025): 117623, https://doi.org/10.1016/j.bios.2025.117623.

61. A. G. Ayankojo, R. Boroznjak, J. Reut, and V. Syritski, "Non-Invasive Electrochemical Detection of Cortisol in Artificial Sweat Using Molecularly Imprinted Polymer," *Talanta* 307 (2026): 129790, https://doi.org/10.1016/j.talanta.2026.129790.

62. S. Cho, S. Shajari, Y. R. Xiong, et al., "Wearable Lateral Flow Assays for Cortisol Monitoring With Time-Dynamic Sweat Sampling and Sensing by Electrochromic Timers," *Nature Sensors* 1 (2026): 85–98, https://doi.org/10.1038/s44460-025-00005-z.

Supporting Information

Additional supporting information can be found online in the Supporting Information section.

Supporting File: adma75671-sup-0001-SuppMat.docx.

15214095, 0, Downloaded from https://advanced.onlinelibrary.wiley.com/doi/10.1002/adma.75671 by Zhi Zhang - Peking University , Wiley Online Library on [23/11/2026]. See the Terms and Conditions (https://onlinelibrary.wiley.com/terms-and-conditions) on Wiley Online Library for rules of use; OA articles are governed by the applicable Creative Commons License